Redox Biology 26 (2019) 101260

Contents lists available at ScienceDirect

Redox Biology

journal homepage: www.elsevier.com/locate/redox

Ammonia sensitive SLC4A11 mitochondrial uncoupling reduces glutamine induced oxidative stress

Diego G. Ogando[1], Moonjung Choi[1], Rajalekshmy Shyam, Shimin Li, Joseph A. Bonanno[*]

Indiana University, School of Optometry, Bloomington, IN, 47405, United States

ARTICLE INFO

Keywords:
Slc4a11
Glutamine
Ammonia
Reactive oxygen species
Mitochondrial uncoupling

ABSTRACT

SLC4A11 is a NH_3 sensitive membrane transporter with H^+ channel-like properties that facilitates Glutamine catabolism in Human and Mouse corneal endothelium (CE). Loss of SLC4A11 activity induces oxidative stress and cell death, resulting in Congenital Hereditary Endothelial Dystrophy (CHED) with corneal edema and vision loss. However, the mechanism by which SLC4A11 prevents ROS production and protects CE is unknown. Here we demonstrate that SLC4A11 is localized to the inner mitochondrial membrane of CE and SLC4A11 transfected PS120 fibroblasts, where it acts as an NH_3-sensitive mitochondrial uncoupler that enhances glutamine-dependent oxygen consumption, electron transport chain activity, and ATP levels by suppressing damaging Reactive Oxygen Species (ROS) production. In the presence of glutamine, *Slc4a11*$^{-/-}$ (KO) mouse CE generate significantly greater mitochondrial superoxide, a greater proportion of damaged depolarized mitochondria, and more apoptotic cells than WT. KO CE can be rescued by MitoQ, reducing NH_3 production by GLS1 inhibition or dimethyl αKetoglutarate supplementation, or by BAM15 mitochondrial uncoupling. *Slc4a11* KO mouse corneal edema can be partially reversed by αKetoglutarate eye drops. Moreover, we demonstrate that this role for SLC4A11 is not specific to CE cells, as SLC4A11 knockdown in glutamine-addicted colon carcinoma cells reduced glutamine catabolism, increased ROS production, and inhibited cell proliferation. Overall, our studies reveal a unique metabolic mechanism that reduces mitochondrial oxidative stress while promoting glutamine catabolism.

The amino acid glutamine (Gln) plays an essential role as both a cellular building block and flexible fuel that supports mitochondrial metabolism. Depending on the cellular metabolic state, Gln can be used as either biosynthetic precursor (e.g., proteins; nucleotides; glutathione) or as an anaplerotic fuel that drives mitochondrial ATP production. As a result of this dual function, Gln is essential in the proliferation and maintenance of many cell types, including the intestinal mucosa, activated lymphocytes, kidney tubules, many cancer cells [1] and the corneal endothelium [2]. However, a major drawback of relying on Gln for ATP production is that catabolism of this amino acid generates ammonia, a potentially toxic metabolic waste product [3,4]. Glutaminase (GLS1 and GLS2) catalyzes the conversion of Gln to Glutamate (Glu) and NH_3 while Glutamate Dehydrogenase (GLUD) catalyzes the conversion of Glu and $NADP^+$ to α-ketoglutarate, NADPH, and NH_3. Gln catabolism can damage mitochondria due to Reactive Oxygen Species (ROS) produced from an energized Electron Transport Chain (ETC) and from direct action of NH_3 on Complexes I and III [5–7]. Therefore, cells that catabolize high levels of Gln must ensure that NH_3 buildup does not interfere with mitochondrial function.

Corneal Endothelium (CE) has a very high density of mitochondria, second in the body only to photoreceptors [8], in order to fulfill the energy requirements of continuous active transport that is required for maintaining corneal hydration [9]. CE meets these energetic demands by generating ATP from both glucose and Gln, with each fuel source accounting for ~50% of TCA cycle intermediates [2]. In the absence of Gln, CE cells experience a significant drop in steady state ATP and decreased CE transport function [2]. The ability of CE to maintain such high levels of Gln catabolism relies, in part, on SLC4A11, an NH_3 activated electrogenic H^+ transporter [10,11]. Mouse Corneal Endothelial Cells (MCEC) derived from the *Slc4a11* KO showed significantly reduced percentages of TCA cycle intermediates originating from Gln [12] indicating that Slc4a11 is facilitating Gln catabolism and as such, influencing mitochondrial function. Moreover, disruptions of SLC4A11 *in vivo* have significant physiological consequences, as mutations in this gene produce Congenital Hereditary Endothelial Dystrophy (CHED), an autosomal recessive disorder that presents

* Corresponding author.
E-mail address: jbonanno@indiana.edu (J.A. Bonanno).
[1] Contributed Equally.

https://doi.org/10.1016/j.redox.2019.101260
Received 10 May 2019; Received in revised form 7 June 2019; Accepted 21 June 2019
Available online 23 June 2019

significant corneal edema and loss of CE cells within the first decade of life [13]. In addition, *Slc4a11*$^{-/-}$ (KO) mice recapitulate CHED [14] along with an increase in corneal endothelial oxidative damage, a hallmark of corneal endothelial dystrophies [15,16]. Similarly, multifactorial late onset Fuchs Endothelial Corneal Dystrophy is also associated with either decreased SLC4A11 expression or dominant mutations in this gene [17–19]. Overall, these results indicate that SLC4A11 maintains CE function and raises the question of how this transporter coordinately regulates Gln catabolism and mitochondrial energy production.

One clue to how SLC4A11 influences metabolism can be derived from electrophysiological analysis, which demonstrate that under physiological conditions, H^+ flux through SLC4A11 is driven inward by the negative membrane voltage [11,20,21]. Patch-clamp studies indicated that NH_3, but not pH or NH_4^+, increased the rate of H^+ influx through SLC4A11 in a concentration-dependent manner, suggesting the possibility of an NH_3–H^+ cotransport model for SLC4A11 [10]. However, an NH_3 activated H^+ flux could not be excluded and studies using Xenopus oocytes suggested that mouse *Slc4a11* is an ideally selective H^+/OH^- conductive pathway, not linked to cotransport of any ion [20]. Overall, these observations indicate that SLC4A11 acts as an NH_3-activated H^+ transporter and raises the possibility that this protein could regulate mitochondrial membrane potential. Not only are the transport properties of SLC4A11 well-suited for a mitochondrial environment (i.e., alkaline pH leading to high glutamine-dependent [NH_3]), but if this transporter was located within the inner mitochondrial membrane, it could provide an NH_3 sensitive H^+ influx that is akin to a mitochondrial uncoupler. Moreover, by functioning as a mild mitochondrial uncoupler, SLC4A11 could reduce ROS generation during periods of high Gln catabolism [22,23], thus serving to protect mitochondria from high [NH_3] and ETC activity.

1. Results

As a first step towards testing this model, we examined mitochondria for the presence of SLC4A11. We found that SLC4A11 is present in mitochondria as shown by immunofluorescence colocalization with MitoTracker in HCEC (Human Corneal Endothelial Cells) (Fig. 1A) and Western analysis of isolated mitochondria in MCEC, HCEC (Fig. 1B) and PS120 fibroblasts stably transfected with HA-tagged SLC4A11 (Fig. 1C), consistent with previous reports of multiple cytoplasmic locations in addition to the plasma membrane [11,24]. TEM immunochemistry of isolated mitochondria from PS120-hSLC4A11-HA cells (Fig. 1D) indicates an inner membrane localization relative to the Outer Mitochondrial Membrane (OMM) marker TOM20. Using a biochemical approach, we treated isolated mitochondria from HCEC and PS120-hSLC4A11-HA transfected cells with increasing amounts of digitonin at 4 °C for 30 min followed by centrifugation, and Western blot of supernatant and pellet (Supplementary Figs. 1A and B), expecting first OMM proteins then IMM proteins in the supernatant relative to the pellet as the [digitonin] increased. The supernatant/total protein ratio as a function of [digitonin] for SLC4A11, the OMM markers VDAC and TOM20, and the IMM markers TIM23 and UCP2 for HCEC (Fig. 1E) and PS120-hSLC4A11-HA (Fig. 1F) reveals that TOM20 and VDAC are released from mitochondria first, followed by TIM23 and UCP2. The supernatant/total SLC4A11 ratio is most closely linked to UCP2, consistent with an inner membrane localization for SLC4A11.

For functional verification of mitochondrial uncoupling, *Slc4a1*1 WT and KO MCEC, grown in Complete Media (OptiMEM with 8% serum and 4 mM L-Alanyl-glutamine, see Methods), and freshly dissected corneal endothelium from WT and KO mice were washed with a HEPES buffered ringer and perfused with TMRE to measure relative changes in Mitochondrial Membrane Potential (MMP). MMP depolarized with increasing [NH_4Acetate] in WT MCEC, but not in KO (Fig. 2A). Similarly, TMRE perfused freshly dissected WT mouse corneal endothelium showed significantly greater NH_4Acetate induced MMP depolarization than KO (Fig. 2B), which is expected if Slc4a11 is an inner membrane NH_3 activated uncoupler. Since mitochondrial uncoupling increases oxygen consumption, we next used Seahorse XF oxygen consumption response analysis to determine if Slc4a11 enhanced Gln-dependent oxygen utilization and was providing a mitochondrial proton leak. First, in the absence of Gln, basal, and ATP-linked respiration were slightly, but significantly, higher in KO vs. WT MCEC, whereas maximal OCR, proton leak, and spare respiratory capacity were not significantly different (Fig. 3 A & B). However, incubation with glucose + Gln increased all OCR parameters significantly more in WT. Most importantly, proton leak was significantly higher in WT in the presence of Gln consistent with Slc4a11 mediated NH_3-sensitive uncoupling. SLC4A11 transfected PS120 fibroblasts, which have a low endogenous level of Slc4a11 [10], also show significantly increased Gln-dependent OCR, spare respiratory capacity, and proton leak (Fig. 3C and D). Consistent with reduced OCR, NH_3 production (glutaminolysis) by KO MCEC in Gln is significantly reduced (Fig. 3E). Moreover, *Slc4a11* CRISPR KD in HCEC reduced NH_3 production and basal OCR in Gln (Fig. 3F &G).

Facilitation of Gln catabolism by Slc4a11 energizes the ETC as indicated by significantly higher NAD/NADH ratio in WT vs KO cells in Gln, whereas in the absence of Gln NAD/NADH ratios are similar over 24 h (Fig. 4A). Interestingly, the total NAD pool is similar in WT and KO in the absence of Gln, but in Gln total NAD is significantly depleted in KO cells, suggesting a secondary consumption of NAD, possibly due to oxidative damage [25]. The Gln-dependent NAD/NADH ratio increase in WT is blocked by Antimycin-Rotenone confirming that it is due to accelerated ETC activity (Fig. 4B). Consistent with the increased OCR and NAD/NADH ratio, 24 h incubation in Gln increased steady-state [ATP] in WT, but decreased [ATP] in KO (Fig. 4C), suggesting that Gln damages KO mitochondria. Conversely, steady-state [ATP] was significantly higher in KO in the absence of Gln, consistent with the higher ATP-linked OCR (Fig. 3A and B) and adaptation to glucose utilization in *Slc4a11* KO cells [12]. In summary, Slc4a11 provides NH_3-dependent mitochondrial uncoupling that facilitates Gln catabolism, which increases ETC activity, respiration, and [ATP].

In the absence of Gln, robust OCR, [ATP], and NAD/NADH parameters in KO relative to WT MCEC suggest similar ETC capacity. CHED patient specimens and mouse KO corneal endothelium are chronically exposed to 0.5 mM Gln *in vivo* [26] and both show significant oxidative damage [15]. An energized ETC and the presence of NH_3 are ideal conditions for ROS production, which could produce mitochondrial dysfunction [27], suggesting that ROS mediated mitochondrial damage limits Gln utilization in KO over time. To determine if Gln usage increases ROS production, *Slc4a1*1 WT and KO MCEC, grown in Complete media were washed with an Assay media that contained DMEM (see Supplementary Table 2 for list of amino acids), 0.5% dialyzed-serum, 5.5 mM glucose, and ± 0.5 mM glutamine for 24 h. In the absence of Gln, WT and KO had similar cellular ROS levels, whereas addition of Gln increased ROS more than 2-fold in KO cells, but had little effect on WT (Supplementary Fig. 2A). This is consistent with a previous report showing that knockdown of SLC4A11 in HCEC increased ROS levels [15]. Similarly, in Complete Media (containing 4 mM L-Alanyl-Glutamine) mitochondrial ROS, expressed as %MitoSOX$^+$ cells, was significantly higher in KO (Fig. 5A-time zero & Supplementary Fig. 2B) and continuously increased in assay media in both WT and KO cells catabolizing Gln. Whereas %MitoSOX$^+$ WT cells increased modestly in the absence of Gln, it decreased significantly in KO cells (Fig. 5A), such that after 24 h, there were > 3x more MitoSOX$^+$ KO cells in Gln relative to no Gln, while there were only 1.3x more MitoSOX$^+$ WT cells in Gln relative to no Gln. These data show that absence of Gln relieves oxidative stress in KO cells, consistent with a preferred use of glucose in *Slc4a11* deficient MCEC [12]. Oxidative damage is greatest in KO corneal endothelium and MCEC in the presence of Gln (Supplementary Figs. 2C and D). Mitochondrial morphology imaged in freshly dissected corneal endothelium from the *Slc4a1*1 WT and KO mice showed a

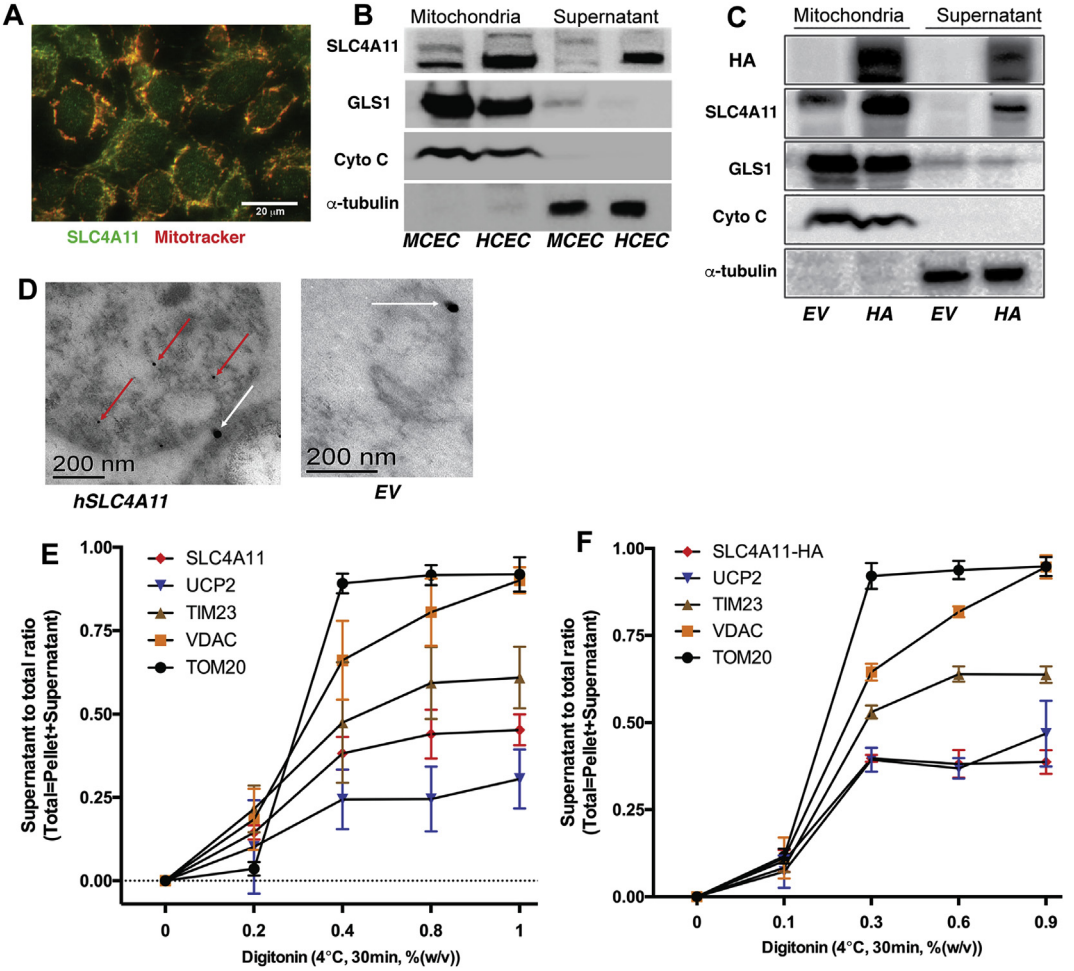

Fig. 1. SLC4A11 Localizes in the Inner Mitochondrial Membrane. (A) Colocalization of SLC4A11 (green) with Mitotracker Red CMXRos in Human Corneal Endothelial Cells (HCEC). **(B)** Western blot of mitochondrial and supernatant fractions from HCEC and Mouse Corneal Endothelial Cells (MCEC) and **(C)** from PS120 fibroblasts transfected with Empty Vector (EV) or hSLC4A11-HA. **(D)** Transmission Electron Microscopy immunostaining of mitochondria with hSLC4A11-HA 10 nm gold (red arrows) and TOM20 25 nm gold (White arrows) antibodies. **(E)** Isolated mitochondria from HCEC and **(F)** PS120-hSLC4A11 were suspended and subjected to different concentrations of digitonin at 4 °C for 30 min, pelleted, supernatant collected and pellet lysed. Western blots of each fraction were probed for HA-tagged SLC4A11, OMM markers TOM20 and VDAC, and IMM markers UCP2 and TIM23 (Supplementary Fig. 1A &B). Release of proteins to the supernatant is plotted as ratio of density of supernatant to total (pellet + sup) band density vs. [Digitonin] (note non-linear scale), n = 3, ± SEM. (For interpretation of the references to color in this figure legend, the reader is referred to the Web version of this article.)

reduced number of mitochondrial networks and branches per network in KO relative to WT (Supplementary Fig. 2E). In addition, increased mito/genomic DNA ratio (Supplementary Fig. 2F), and association of mitochondria with lysosomes (Supplementary Fig. 2G) in KO MCEC *in vitro* indicate greater rates of mitochondrial turnover. In this regard, we examined the effect of Gln on autophagy flux by measuring LC3b levels in the presence and absence of Gln and the lysosomal H^+-ATPase inhibitor Bafilomycin A1, a downstream inhibitor of autophagy [28]. Gln catabolism induced a 64% increase in autophagy flux in KO cells and only a 6% increase in WT (Supplementary Fig. 2H). These results show that Gln catabolism in corneal endothelium induces damaging mitochondrial ROS and increased autophagy that is suppressed by Slc4a11.

A potential consequence of mitochondrial damage and prerequisite for mitophagy is MMP collapse. In complete media, MCEC *Slc4a11* KO cells have significantly reduced numbers of polarized mitochondria, expressed as %TMRE positive stained cells relative to WT (Fig. 5B, time zero; Supplementary Fig. 3). Fig. 5B also shows that incubation in assay media with Gln over time reduces the number of polarized mitochondria in both WT and KO, indicating that Gln catabolism is stressful. Conversely, incubation in the absence of Gln shows an increase in the numbers of polarized mitochondria in KO cells and no change in WT, which parallels the decrease in KO levels of mitochondrial superoxide under this condition (Fig. 5A). Within the $TMRE^+$ population we calculated the geometric mean fluorescence, which is a relative measure of MMP. The geometric mean increases in Gln over time (Fig. 5C), indicating that as the $TMRE^+$ population shrinks, the MMP is becoming more hyperpolarized within this population. This hyperpolarization is significantly greater in KO cells. After 24 h incubation, the $TMRE^+$ geometric mean of KO cells in Gln was 80% greater than WT, indicating that KO cell mitochondria became significantly more hyperpolarized than WT (Fig. 5C). In sum, we are finding that Gln, feeding into the TCA cycle, energizes the ETC exerting a hyperpolarizing force on MMP, which is offset by SLC4A11 uncoupling. Excessive hyperpolarization in KO mitochondria in response to Gln drives ROS increases (see also [29]), which damage relatively more mitochondria that then lose polarization (i.e. the $TMRE^-$ population). This scenario leads to lower ATP levels and a greater propensity toward apoptosis. Fig. 5D shows that the %Annexin-V^+ populations in both WT and KO are essentially unchanged after 24 h incubation in assay media without Gln, whereas Gln induces a significantly greater increase in %Annexin-V^+ cells in KO, which again indicates the stress induced by Gln catabolism.

If mitochondrial ROS is causing dysfunction and MMP hyperpolarization is a driver of ROS, then either reducing mitoROS levels directly

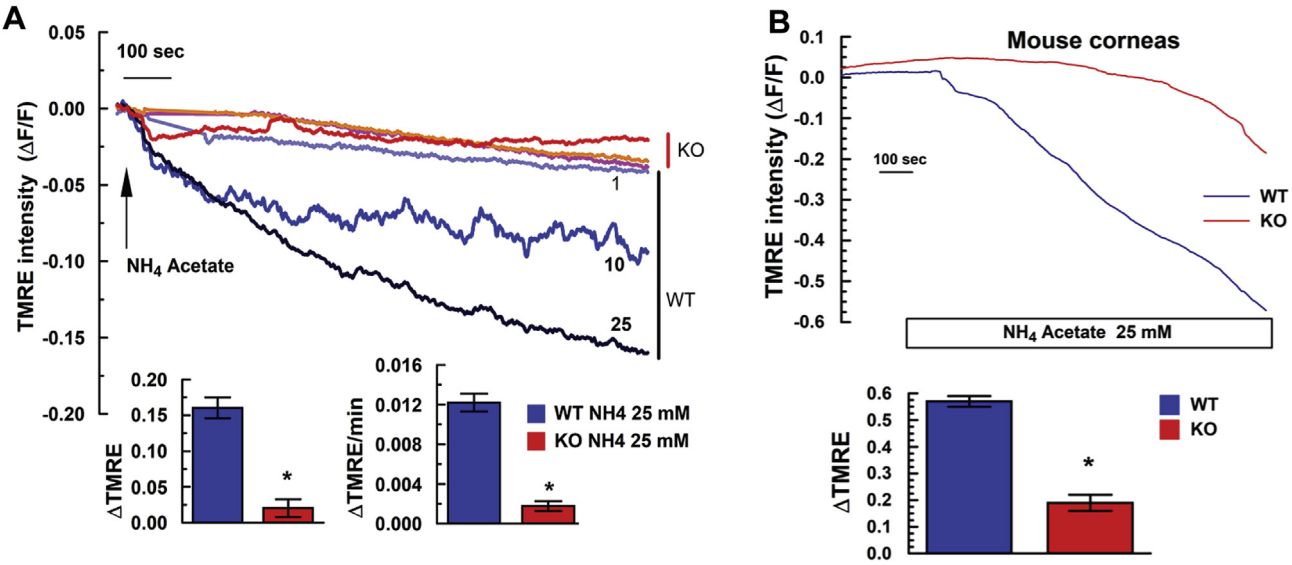

Fig. 2. NH_3 Induced MMP Depolarization. (A) MCEC (WT and *Slc4a11* KO) were loaded with 30 nM TMRE for 30 min then perfused in a HEPES buffered ringer with 10 nM TMRE. After stabilization 1, 10, or 25 mM NH_4Acetate was added. Wild type responses (blue and black traces labelled 1, 10, and 25) showed decreased fluorescence (ΔF/F) indicating depolarization of MMP while KO cells (red traces) showed little depolarization at any [NH_4Acetate]. Bar graph indicates total TMRE fluorescence change and rate of change, n = 3, *p < 0.05. **(B)** Endothelial cell surface of WT and KO corneas from 12 week old mice were loaded with 30 nM TMRE for 30 min and perfused with 10 nM TMRE. After stabilization, corneas were exposed to 25 mM NH_4Acetate.Top-Average time trace of TMRE fluorescence, Bottom bar graph- Maximum change, n = 3, *p < 0.05. (For interpretation of the references to color in this figure legend, the reader is referred to the Web version of this article.)

or decreasing MMP hyperpolarization should rescue *Slc4a11* KO cells. The thiol redox state buffer N-Acetylcysteine (10 mM) was ineffective, however MitoQ significantly reduced Gln-induced apoptosis in KO cells (Fig. 5E) while lowering Mitochondrial ROS (Fig. 5F). MitoQ also increased the number of polarized mitochondria (Fig. 5G) and significantly elevated ATP levels in KO populations (Fig. 5H). Next, we decreased MMP hyperpolarization with the mitochondrial uncoupler BAM15 [30]. Fig. 6A shows that BAM15 (1 μM) increased apoptosis in WT and KO cells in glucose only. Conversely, BAM15 completely inhibited Gln-induced apoptosis in WT and KO cells. In KO cells exposed to Gln, BAM15 eliminated the excessive mitoROS production, increased the number of polarized mitochondria and reduced the excessive hyperpolarization (Fig. 6A–D). Whereas in the absence of Gln, BAM15 uncoupling reduced the %TMRE$^+$ WT and KO population and MMP was less polarized within this population (Fig. 6C and D), as expected for an uncoupler. Moreover, KO cells exhibited a small expected drop in [ATP] when incubated with BAM15 in glucose alone, but full [ATP] restoration in Gln (Fig. 6E). Finally, BAM15 uncoupling restored KO OCR to WT levels (Fig. 6F), which is consistent with other studies showing that modest FCCP uncoupling can increase Gln-dependent oxygen consumption [31]. Overall, KO cells exposed to BAM15 in the absence of Gln exhibited the expected depressive effects on mitochondria, but in the presence of Gln, BAM15 uncoupling reduces hyperpolarization driven ROS production, improves respiration and prevents Gln-induced KO cell apoptosis. This result is consistent with BAM15 rescuing the mitochondrial defects associated with loss of SLC4A11 uncoupling.

In conjunction with an energized ETC, Gln-derived NH_3 can increase ROS through interactions with Complex I and III [5,6]. Gln (0.5 mM) increases total extracellular NH_3 (NH_4^+ + NH_3) to 0.4–0.6 mM after 24 h, when WT [NH_3] is 1.5-fold higher than KO (Fig. 3E). To test if NH_3 can directly harm MCEC, WT and KO cells were incubated for 24 h in the absence of Gln, but with increasing [NH_4Acetate]. We found that KO cells showed a 2.4-fold increase in apoptosis at 25 mM, whereas WT cells were resistant (Fig. 7A). These data show that *Slc4a11* KO cells are more sensitive to the toxic effects of NH_3 than WT cells. Twenty-four hours incubation with 25 mM NH_4Acetate, induced a 2-fold increase in %MitoSOX$^+$ cells in KO, with no significant effect in WT (Fig. 7B). Concomitantly, NH_3 significantly reduces the number of polarized mitochondria in KO, but not WT cells (Fig. 7C). Similarly, [ATP] is unaffected by NH_3 in WT, but reduced by 4-fold in KO cells (Fig. 7D). Overall, these results indicate that SLC4A11 is facilitating Gln catabolism by suppressing the damaging effects of an energized ETC and NH_3, consistent with other studies showing that high [NH_3] induces mitochondrial ROS and dysfunction in glia, neurons, heart and skeletal muscle by interaction with ETC components [5–7,32–34].

We next examined the potential of reducing Gln-dependent NH_3 production or scavenging NH_3 to reduce ROS and protect KO cells. We attempted to dampen NH_3 levels in KO cells by treating them with either a permeable form of pyruvate (Methyl-pyruvate; MP), which undergoes a transamination reaction with NH_3 to form alanine [35], or with dimethyl-α-ketoglutarate, which reduces NH_3 production by slowing Gln catabolism (Fig. 8A). We found that MP did not reduce [NH_3], while Dimethyl-αKG reduced [NH_3] to control levels in both WT and KO (Fig. 8B). Consistent with these observations, MP had no protective effect, but Dimethyl-αKG completely reduced %Annexin-V$^+$ to control levels (Fig. 8C). Furthermore, inhibitors of Glutaminase-1, 20 μM BPTES and 10 μM CB839, partially reduced Gln-induced NH_3 production in WT and in KO cells (Fig. 8D), completely protected WT cells, and significantly decreased %Annexin-V$^+$ in KO cells (Fig. 8E). Decreasing [NH_3] in KO cells by Dimethyl-αKG or Gls-1 inhibition also increased the number of polarized KO cell mitochondria, decreased superoxide production, and increased [ATP] in KO cells (Fig. 8F, G, & H). In contrast, Gls-1 inhibition of WT cells although mildly protective, reduced steady-state [ATP], as expected for Gls1 inhibition. The complete protection of KO cells by Dimethyl-αKG relative to the partial protection by Gls1 inhibition is consistent with the reductions in NH_3 production and corroborates the damaging effects of NH_3.

Given the dramatic rescue of *Slc4a11* KO cells by Dimethyl-αKG *in vitro* and the potential *in vivo* utility as a small molecule nutritional supplement, we supplied Dimethyl-αKG to 12 week old *Slc4a11* KO mice by topical eye drops. Because of the short duration of exposure and the need to penetrate corneal layers to reach the endothelium, we used eyedrops with 10x the concentration used *in vitro*. Fig. 9A shows

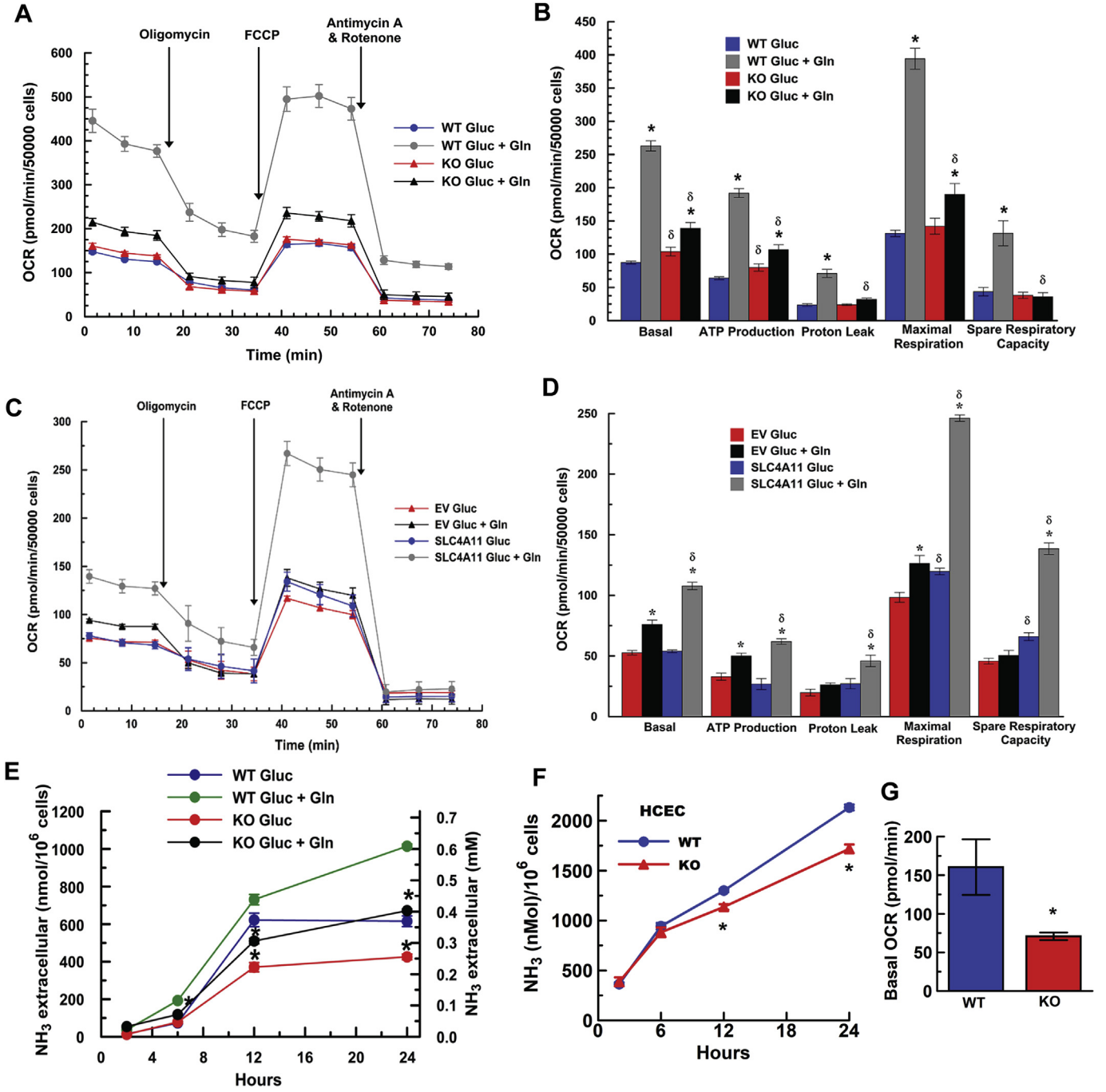

Fig. 3. Gln Induced Oxygen Consumption and Ammonia Production. (A) Seahorse XF Oxygen Consumption Response in Mito Stress Test. MCEC in complete media were preincubated for 45 min at 37 °C (in the absence of CO_2) in XF Base Medium containing 14 mM glucose ± 4 mM Gln, then placed into Seahorse analyzer. Basal OCR was followed by ATP related OCR (2 μM oligomycin), then complete uncoupling to give Maximum OCR (0.5 μM FCCP), followed by ETC blockade (0.5 μM Antimycin A and 0.5 μM Rotenone). **(B)** Summary of results from (A), n = 3, ± SEM, *p < 0.05 vs Glucose for same genotype; δ:p < 0.05 vs WT, for same treatment. **(C & D)** OCR trace and summary results of hSLC4A11 over-expressing PS120 fibroblasts. n = 3, *p < 0.05 vs Gluc, same genotype. δ: p < 0.05 vs EV; EV-Empty Vector. **(E)** Ammonia production in DMEM assay media (0.5% dialyzed-serum) with glucose or glucose + 0.5 mM glutamine in *Slc4a11* WT and KO MCEC, n = 3 for each condition, *p < 0.05 less than WT for same condition. **(F)** Effect of CRISPR KD of SLC4A11 in HCEC on Ammonia production and **(G)** Basal OCR in Gln; n = 3, *p < 0.05.

that one drop of 50 mM Dimethyl-αKG (0.87%) three times per day significantly reduced corneal edema (Supplementary Fig. 4A) in KO mice over 28 days, whereas osmotically balanced vehicle or αKG drops with WT mice had no effect. This partial reversal of corneal edema in the KO by αKG validates the *in vitro* metabolic model and offers a potential clinical medical therapy approach, in addition to corneal transplantation, for CHED.

A recent report comparing normal and glutamine-addicted cancerous ovarian tissues found that high expression of SLC4A11 is an independent predictor of poor survival [36], suggesting that SLC4A11 may be facilitating Gln consumption and minimizing ROS production in glutamine addicted cancer cells, as well. We found that SLC4A11 was highly expressed in HT29 and HCT116 Gln-addicted colon carcinoma cell lines (Supplementary Fig. 4B). Transient knockdown of SLC4A11 (~50% between 48-72 h, Supplementary Fig. 4C) reduced Gln-dependent NH_3 production, increased mitoROS (Fig. 9B and C), and

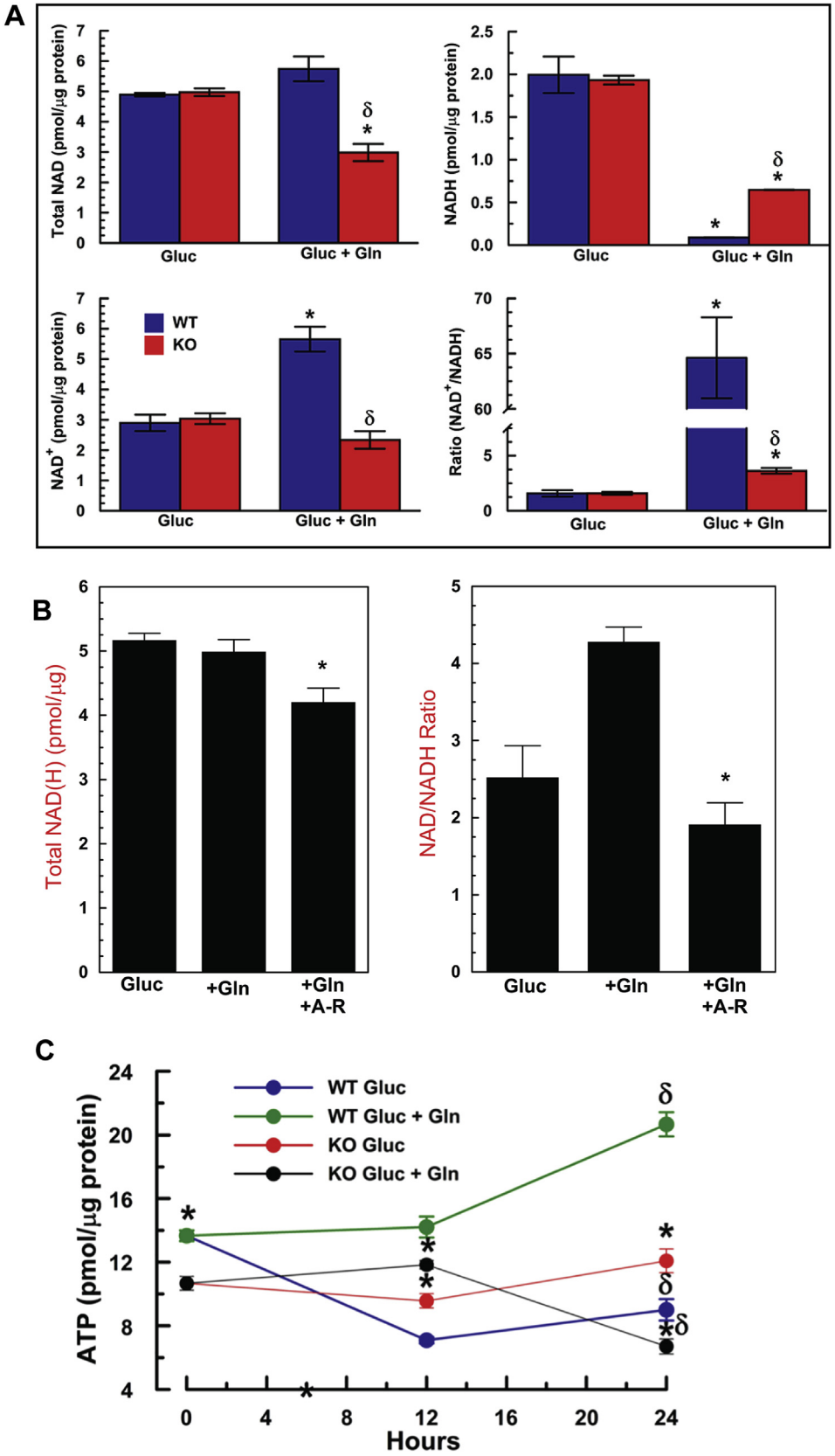

Fig. 4. Gln Accelerates ETC Activity. (A) MCEC WT and KO were incubated in assay media ± 0.5 mM glutamine for 24 h, washed and analyzed for NAD and NADH; n = 3, *p < 0.05 vs Gluc, same genotype. δ: p < 0.05 vs WT. **(B)** WT MCEC incubated for 4 h ± Gln ± 10 μM Antimycin A and 5 μM Rotenone. n = 3, *p < 0.05 ± drugs. **(C)** Effect of 0.5 mM Gln on [ATP] in WT and KO MCEC. n = 3, *p < 0.05 vs WT. δ: p < 0.05 at 24 vs zero hours.

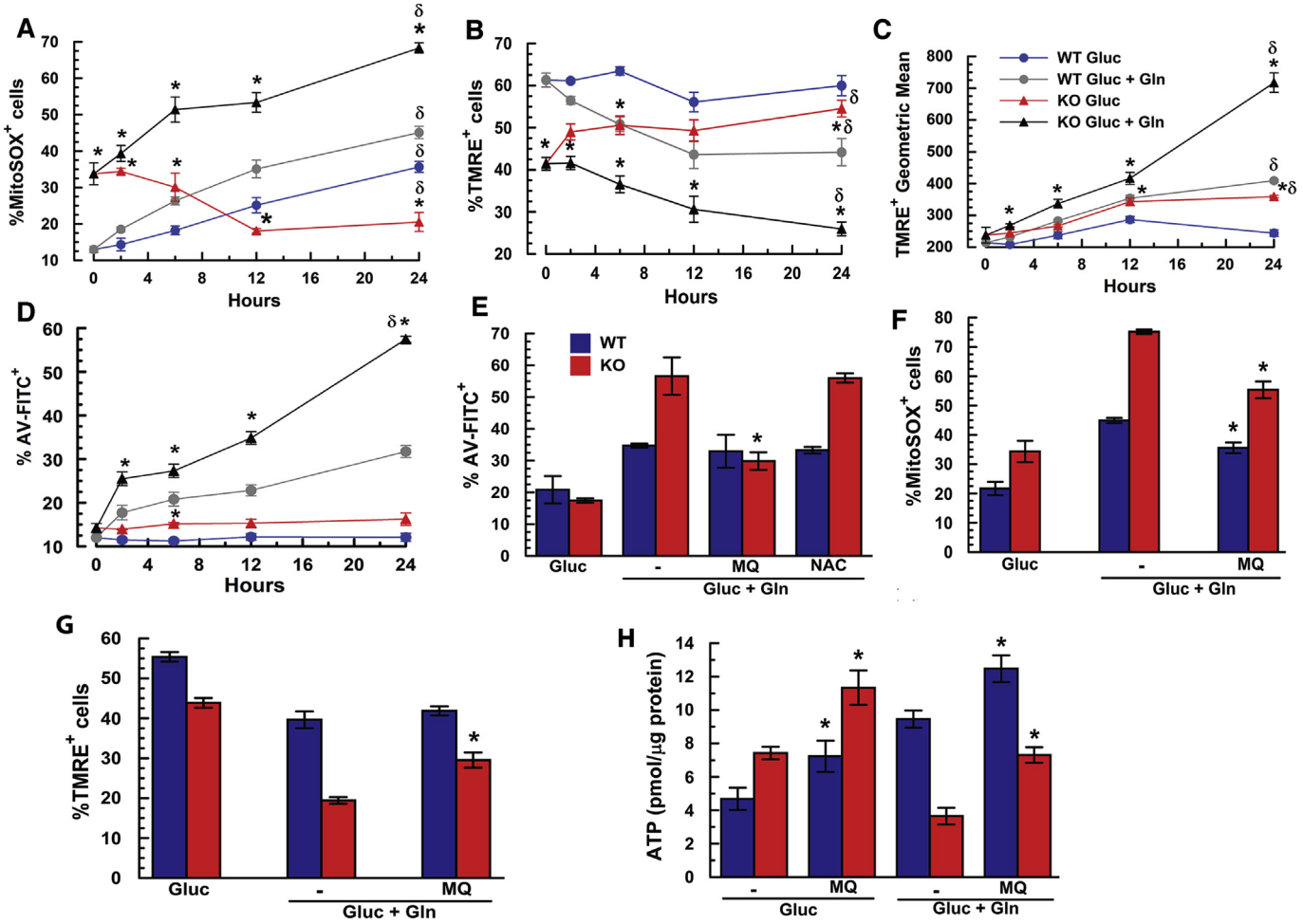

Fig. 5. Slc4a11 reduces Gln-induced ROS and oxidative damage. (A) Effect of Gln on mitoROS. MCEC WT and KO cells in Complete Media were washed with assay media that contained DMEM (see Supplementary Table 2 for list of amino acids), 0.5% dialyzed-serum, 5.5 mM glucose, and ± 0.5 mM Gln for 2–24 h. Cells were stained for 20 min with 2.5 μM MitoSOX 37 °C, followed by one wash with HBSS and analyzed by flow cytometry into $MitoSOX^+$ or $MitoSOX^-$ populations (see Supplementary Fig. 2B), n = 3, *p < 0.05 vs Gluc, same genotype. δ: p < 0.05 vs WT, same treatment at 24 h. **(B)** Effect of Gln on mitochondrial polarization. MCEC WT and KO were incubated in assay media ± 0.5 mM Gln over 24 h. Cells were stained for 20 min with 100 nM TMRE 37 °C, followed by one wash with HBSS and analyzed by flow cytometry into $TMRE^+$ or $TMRE^-$ populations (see Supplementary Fig. 3), n = 3, *p < 0.05 vs Gluc, same genotype. δ: p < 0.05 vs WT, same treatment at 24 h. **(C)** Hyperpolarization MMP by Gln shown by Geometric mean of $TMRE^+$ population, n = 3, *p < 0.05 vs Gluc, same genotype. δ: p < 0.05 vs WT, same treatment at 24 h. **(D)** Effect of Gln on Apoptosis. MCEC WT and KO were incubated in assay media ± 0.5 mM glutamine over 24 h. Cells were stained with AnV-FITC for 5 min, followed by one wash with HBSS and analyzed by flow cytometry, n = 3, *p < 0.05 vs Gluc, same genotype. δ: p < 0.05 vs WT, same treatment at 24 h. **(E)** Rescue of KO cells by MitoQ. MCEC WT and KO were incubated in assay media +0.5 mM glutamine, and 1 μM MitoQ, or 10 mM N-Acetyl-cysteine (NAC) for 24 h, n = 3, *p < 0.05 ± drug. **(F)** MitoQ reduces Gln-dependent mitoROS, n = 3, *p < 0.05 ± MQ. **(G)** 1 μM MitoQ for 24 h increases $\%TMRE^+$ KO cells, n = 3, *p < 0.05 ± MQ. **(H)** [ATP] in WT and KO MCEC after 24 h n = 3, *p < 0.05 ± MQ.

transiently decreased proliferation in these carcinoma cells (Fig. 9D).

2. Discussion

SLC4A11 acting as an ammonia-sensitive mitochondrial uncoupler is supported by data showing ammonia-induced electrogenic H^+ influx [10,11]; ammonia-induced MMP depolarization in WT, but not KO MCEC & mouse cornea; SLC4A11 localization to the inner mitochondrial membrane; and increased oxygen consumption and Proton Leak in the presence of Glutamine in WT, but not KO MCEC, as well as human corneal endothelial cells and SLC4A11 transfected PS120 fibroblasts. The absence of SLC4A11 leads to: 1) greater sensitivity to the toxic effects of ammonia, 2) significant Gln-induced MMP hyperpolarization with high levels of mitoROS that damage mitochondria, 3) reduced ATP availability, 4) increased mitochondrial turnover, and 5) a greater rate of apoptosis, indicating that SLC4A11 uncoupling reduces the driving force for ROS production caused by an enhanced ETC and the presence of ammonia. These conclusions are consistent with finding that reducing ROS levels directly with MitoQ, by exogenous uncoupling with BAM15, or slowing NH_3 production by GLS1 inhibition or dimethyl-αKetoglutarate protect SLC4A11 deficient cells *in vitro* and can reduce *Slc4a11* KO mouse corneal edema *in vivo*. These results lead to a model of NH_3 activated mitochondrial uncoupling by SLC4A11 as illustrated in Fig. 9E. Cells that are consuming Gln are in a milieu of diffusing NH_3. This activates both plasma membrane and mitochondrial SLC4A11. H^+ influx via SLC4A11 at the plasma membrane lowers pHi [10,11,37], which would support H^+ influx via mitoSLC4A11. SLC4A11 uncoupling lowers the proton motive force, reducing ROS production, protecting the mitochondria and allowing them to catabolize Gln and produce higher ATP levels. Mild uncoupling has been shown to reduce ROS production [22,23], and the reduction of ROS and protection of *Slc4a11* KO cells by BAM15 uncoupling corroborates the hypothesis.

Given the current context of NH_3 toxicity, an NH_3:H^+ cotransport model for SLC4A11 [10] would be counterproductive. Conversely, an antiport configuration could facilitate NH_3 removal from mitochondria

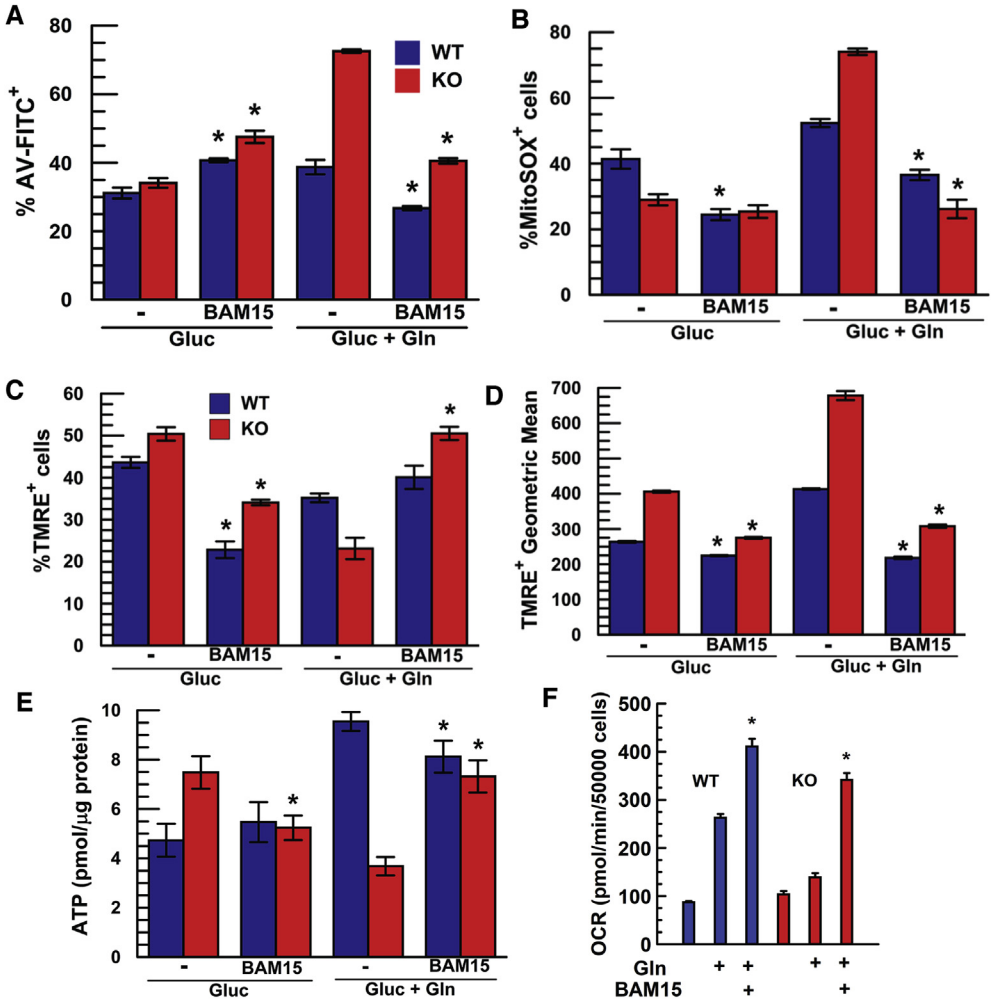

Fig. 6. BAM15 Uncoupling Reverses Detrimental Effects of Glutamine in Slc4a11 KO. (A) %AnV$^+$ WT and KO MCEC incubated in assay media +0.5 mM glutamine, and ± 1 μM BAM15 for 24 h, n = 3, *p < 0.05 ± BAM15. **(B)** BAM15 uncoupling reduces Gln-dependent MitoROS. MCEC WT and KO were incubated in assay media +0.5 mM glutamine, and ± 1 μM BAM15 for 24 h, n = 3, *p < 0.05 ± BAM15. **(C)** %TMRE$^+$ and **(D)** Geometric mean of TMRE$^+$ population of WT and KO MCEC incubated in assay media ± 0.5 mM Gln, and ± 1 μM BAM15 for 24 h then stained with TMRE. **(E)** Restoration of [ATP] in KO MCEC by BAM15 in 0.5 mM Gln, n = 3, *p < 0.05 vs no BAM15 for same genotype. **(F)** Basal Oxygen Consumption in KO rescued by BAM15 uncoupling, n = 3, *p < 0.05 ± BAM15.

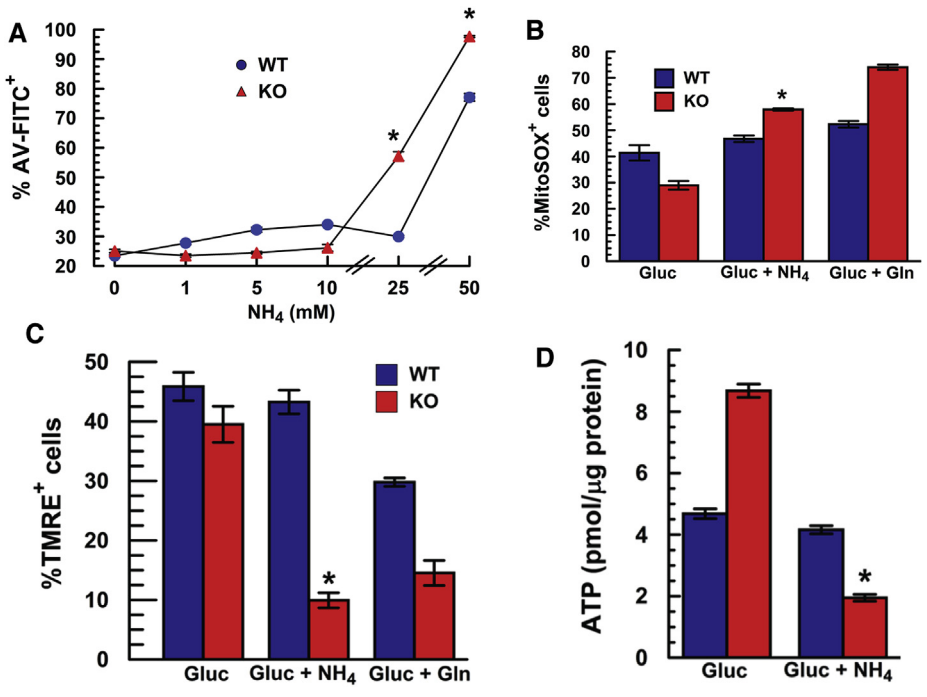

Fig. 7. Detrimental Effect of NH_3 on Apoptosis and MitoROS in MCEC KO cells. (A) Apoptosis vs. [Ammonium Acetate] in Gluc 1 g/L for 24 h, n = 3, *greater than WT p < 0.05. **(B)** Percentage of MitoSOX$^+$ cells following 24 h incubation with 25 mM NH_4Acetate, n = 3 *p < 0.05 vs Gluc; same genotype. **(C)** Effect of 24 h of 25 mM NH_4Acetate on %TMRE$^+$ cells; effect of 0.5 mM Gln shown for comparison, n = 3, *p < 0.05 vs Gluc, same genotype. **(D)** Effect of 24 h of 25 mM NH_4Acetate on [ATP], n = 3, *p < 0.05 vs Gluc, same genotype.

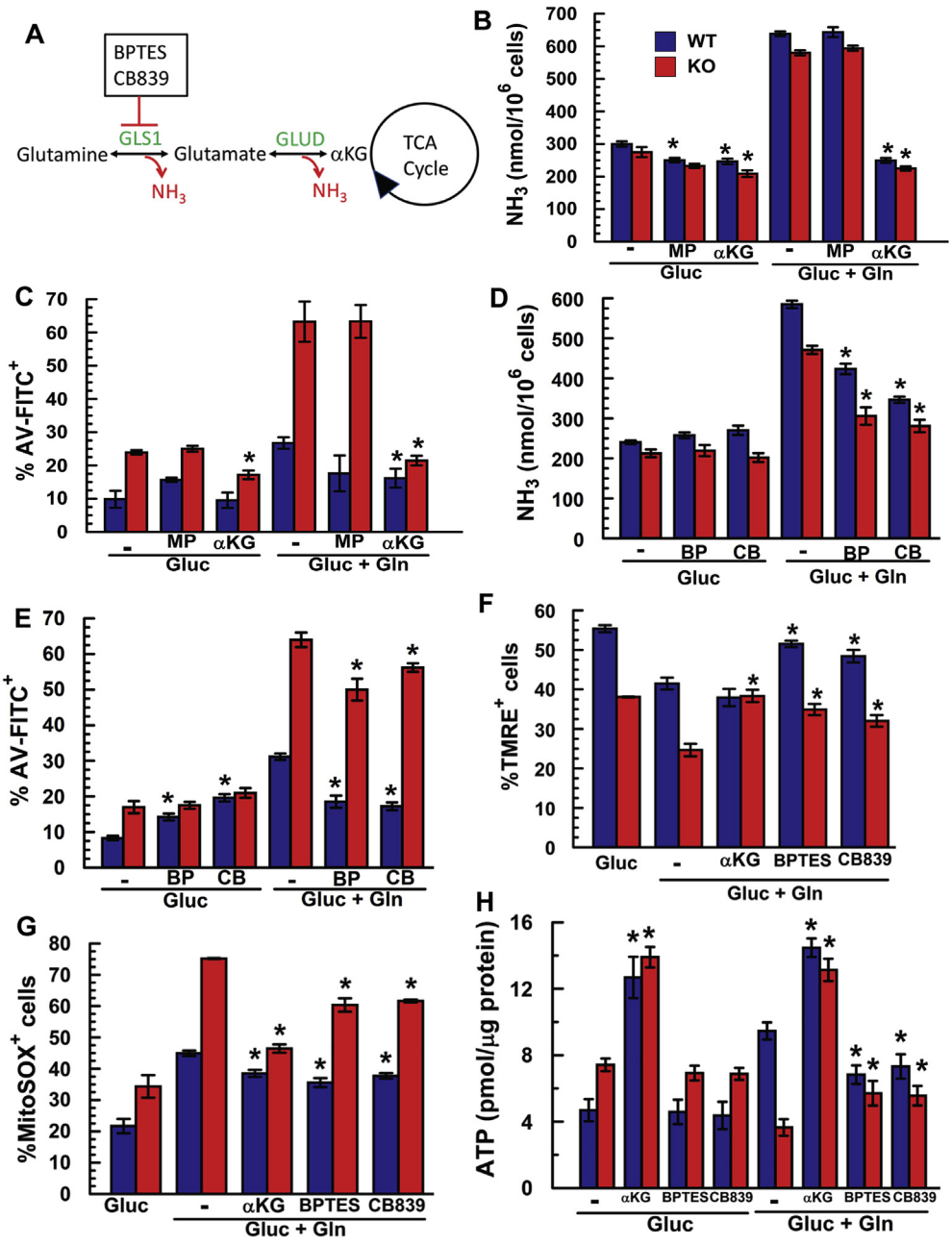

Fig. 8. Slc4a11 KO Rescue by Inhibition of Gln Derived NH_3. **(A)** Illustration of potential reduction of ammonia production by GLS1 inhibitors or presence of excess αKG. **(B)** Extracellular NH_3 production in presence of αKG (5 mM) or MethylPyruvate (5 mM), n = 3, *p < 0.05 ± drug. **(C)** Apoptosis in presence of αKG or MP, n = 3, *p < 0.05 ± αKG. **(D)** Extracellular NH_3 production in presence of GLS1 inhibitors BPTES (20 μM) or CB839 (10 μM), n = 3, *p < 0.05 ± drug. **(E)** Apoptosis in presence of GLS1 inhibitors BPTES or CB839, n = 3, *p < 0.05 ± drug. **(F)** GLS1 inhibition (BPTES & CB839) and αKG supplementation increase %$TMRE^+$ mitochondria. n = 3, *p < 0.05 ± drug. **(G)** GLS1 inhibition and αKG supplementation decreases Gln-induced mitoROS production and **(H)** recovers [ATP], n = 3, *p < 0.05 ± drug.

together with AQP8 facilitated diffusion [38] and passive diffusion of NH_3 gas. The current model suggests and the results are consistent with SLC4A11 being allosterically activated by NH_3 and is consistent with a recent study suggesting that Slc4a11 is an ideally selective H^+/OH^- conductive pathway, uncoupled from cotransport of any ion [20]. While there is consensus that SLC4A11 is an electrogenic H^+ transporter [10,20,39,40], the specific transport configuration(s), mechanism for activation by NH_3, and kinetic properties within mitochondria requires further analysis.

High NH_3 production rates would suggest that there are multiple mechanisms for cell protection in addition to mitochondrial uncoupling. For example, NH_3 can induce autophagy [41–43], which in this context could be protective. Also, a recent study shows that high NH_3 reduces degradation of Hypoxia Inducible Factor (HIF1α) [44] and is protective. Since NH_3 causes oxidative stress, there will also be upregulation of anti-oxidant genes, including SLC4A11, which is upregulated by oxidative stress [15]. Gln consumption will also supply glutamate, increasing total [glutathione] and NADPH, which appears essential in reducing ROS of glutamine-addicted cancer cells [45]. In addition, Gln consumption can potentially induce UCP2 expression [46], which helps shuttle C-4 TCA cycle metabolites to the cytoplasm, leading to increased NADPH levels [47].

SLC4A11 mutations that lead to CHED or some instances of late-onset Fuchs Dystrophy are relatively rare conditions. CHED is often associated with hearing deficits, together known as Harboyan syndrome [48]. Other than the cornea and inner ear, no other deficits in humans have been noted, either because they have not been pursued, are compensated by other gene expression, or are not significant. Close inspection of the OCR data (Fig. 3) reveals that there are two apparent adaptations in *Slc4a11* KO MCEC: higher OCR than WT in the absence of Gln and a small apparent proton leak induced by Gln. The higher OCR is consistent with a greater percentage of TCA cycle intermediates originating from glucose in KO MCEC suggesting more efficient glucose utilization by KO MCEC [12] and is consistent with higher [ATP] in the absence of Gln (Fig. 4C). The small proton leak induced by Gln in KO may be due to higher Ucp2 expression in KO (Supplementary Fig. 4D),

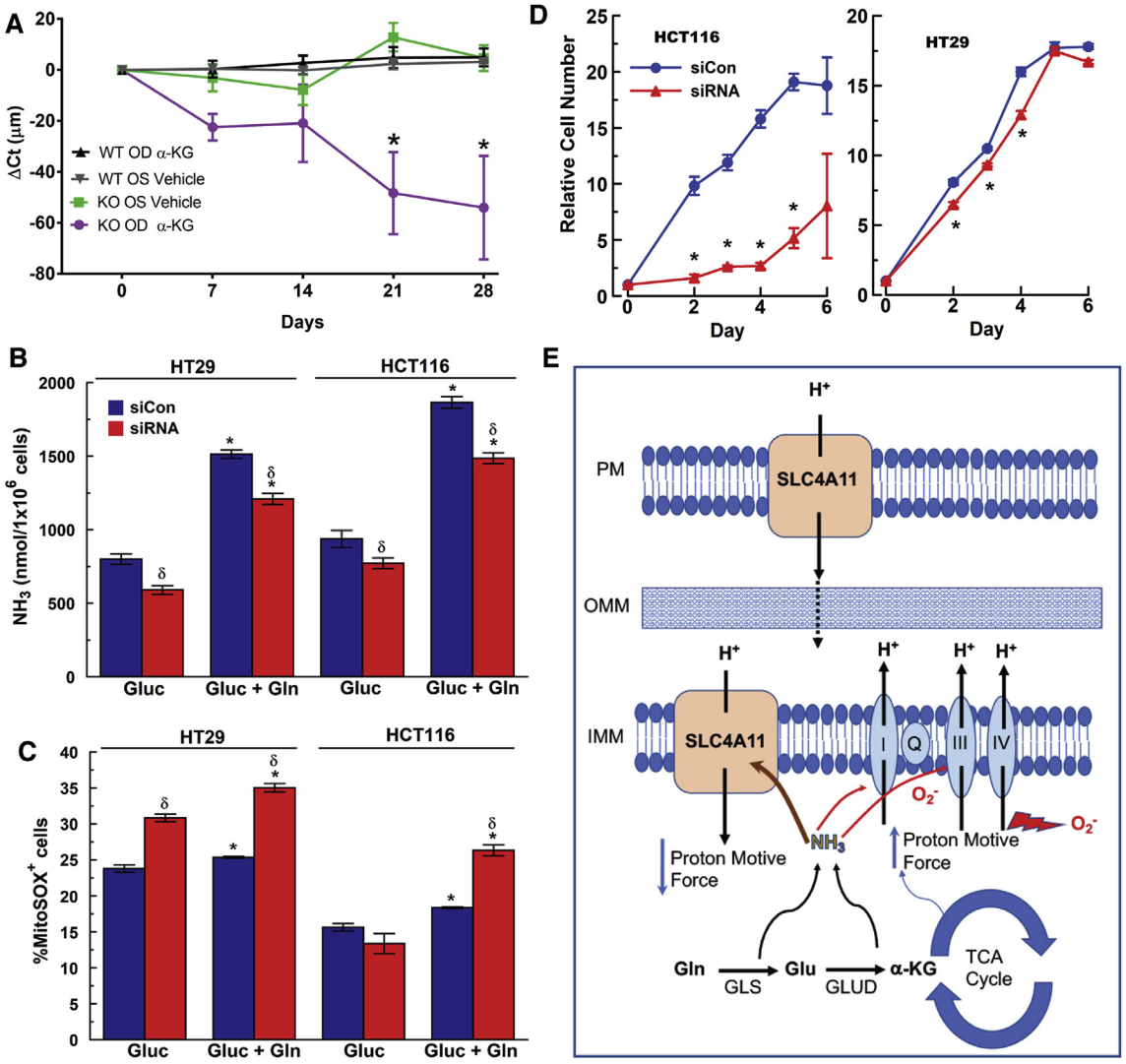

Fig. 9. Rescue of *Slc4a11* KO Mouse, SLC4A11 knockdown in Colon Carcinoma, and Model for Activity. (A) Change in Corneal Thickness (ΔCt) in three WT and three KO mice receiving one drop of 50 mM dimethyl-αKG three times per day over 28 days. Vehicle was Lacripure saline solution osmotically matched with sucrose. *p < 0.05 significantly reduced compared to vehicle. **(B)** Effect of transient siRNA knockdown of SLC4A11 on ammonia production and **(C)** MitoROS in HT29 and HCT116 colon carcinoma cells. Cells were incubated in assay media with 2 mM Glutamine for 24 h. Media was collected for ammonia assay and cells were stained for 20 min with 2.5 μM MitoSOX 37 °C, followed by one wash with HBSS and analyzed by flow cytometry into $MitoSOX^+$ or $MitoSOX^-$ populations. n = 3, *p < 0.05 vs Gluc, same siRNA treatment, δ: p < 0.05 vs Negative siRNA. **(D)** Effect of transient siRNA knockdown of SLC4A11 on HT29 and HCT116 proliferation, n = 3, *p < 0.05, ± SD. **(E)** Model for SLC4A11 function at plasma membrane and inner mitochondrial membrane. Glutamine derived αKG accelerates the TCA cycle and energizes the ETC, which increases the proton motive force and together with [NH_3], increase the production of ROS. Mild uncoupling from NH_3 activated SLC4A11 reduces the proton motive force, lowering ROS production, protecting mitochondria, and facilitating glutamine catabolism.

in that Ucp2 has been shown to provide uncoupling-like activity while enhancing Gln catabolism [47]. Further studies are needed to examine these and other cellular adaptations to SLC4A11 deficiency as well as clinical studies of function in SLC4A11 expressing tissues [49].

Lastly, the EST profile of SLC4A11 suggests high expression in some tumors and increased SLC4A11 expression in ovarian carcinoma indicates a poor survival outcome [36]. Moreover, we found that SLC4A11 is expressed in two "glutamine-addicted" colon carcinoma cell lines suggesting that SLC4A11 is facilitating Gln metabolism in some carcinomas. Using siRNA we found that modest transient knockdown significantly slowed HCT116 and HT29 proliferation, indicating that further studies of the role of SLC4A11 in facilitating Gln catabolism in "glutamine-addicted" carcinomas are needed.

3. Conclusions

SLC4A11 is localized to the inner mitochondrial membrane where it provides mild ammonia-sensitive uncoupling that prevents extreme hyperpolarization during glutamine catabolism. SLC4A11 uncoupling reduces ROS production from an energized ETC and the presence of NH_3, thereby limiting mitochondrial damage and apoptosis. As such, SLC4A11 deficient cells can be rescued in the presence of glutamine by mitochondrial ROS scavenging, BAM15 uncoupling, or reduction in ammonia production, which have the potential for *in vivo* therapy of CHED. Evidence is provided that SLC4A11 may be important in the maintenance and proliferation of some "glutamine-addicted" carcinomas. In sum, our results lead us to predict that mitoSLC4A11 ammonia-activated uncoupling could be associated with protection of any cell type that catabolizes Gln and/or handles large NH_3 concentrations.

4. Materials and methods

4.1. Mouse model

Slc4a11$^{-/-}$ mice [14] were generously provided by Eranga N. Vithana, Singapore Eye Research Institute. All mice were housed and maintained in pathogen-free conditions and used in the experiments in accordance with institutional guidelines and the current regulations of the National Institutes of Health, the United States Department of Health and Human Services, the United States Department of Agriculture and Association for Research in Vision and Ophthalmology (ARVO) Statement for the Use of Animals in Ophthalmic and Vision Research.

4.2. Cell culture experiments

The generation of conditionally immortalized mouse corneal endothelial cells (MCEC) *Slc4a11*$^{+/+}$ and *Slc4a11*$^{-/-}$ is described previously [12]. Cells were cultured in Complete Media, which contains OptiMEM-I medium (#51985; Thermo Fisher Scientific, Canoga Park, CA, USA), 14 mM Glucose and 4 mM L-Alanyl-Glutamine supplemented with 8% heat-inactivated fetal bovine serum (FBS) (#10082139; Thermo Fisher Scientific), EGF 5 ng/ml (#01–107 Millipore, Darmstadt, Germany), pituitary extract 100 μg/ml (Hyclone Laboratories, Logan, UT, USA), calcium chloride 200 mg/L, 0.08% chondroitin sulfate (#G6737; Sigma-Aldrich Corp., St. Louis, MO, USA), gentamicin 50 μg/ml (#15710072; Thermo Fisher Scientific), antibiotic/antimycotic solution diluted 1:100 (#15240062; Thermo Fisher Scientific) and 44 units/mL IFN-γ (#485-MI; R&D Systems, Minneapolis, MN, USA). On the day of experiments cells were incubated in Assay Media, which contained DMEM (no glucose, no glutamine, no sodium pyruvate, no phenol red) (#A14430-01; Thermo Fisher Scientific, Canoga Park, CA, USA), supplemented with glucose 1 g/L (5.5 mM) (#A24940-01, Thermo Fisher Scientific), glutamine (0.5 or 2 mM) (#250030–081, Thermo Fisher Scientific) and 0.5% dialyzed FBS (#26400–036; Thermo Fisher Scientific) at 33 °C for 2–24 h.

Stable transfection of SLC4A11-HA tagged or empty vector (EV) into PS120 Chinese hamster CCL39 fibroblast cell line was generated as described previously [10] and cultured in DMEM (#21063, Thermo Fisher Scientific) supplemented with 5% heat-inactivated FBS (#10082139; Thermo Fisher Scientific, 1% antibiotic/antimycotic (#15240062; Thermo Fisher Scientific) and 1 mg/ml Geneticin G418 (#10131027; Thermo Fisher Scientific) at 37 °C. Immortalized HCEC [50] were cultured in the same medium as MCEC but not supplemented with IFN-γ at 37 °C.

4.3. Immunofluorescence staining

Cells plated on coverslips were incubated with 300 nM MitoTracker Red CMXRos (#M7512, Thermo Fisher Scientific) for 30 min at 37 °C, and then fixed with 100% cold methanol for 10 min at room temperature. The fixed cells were permeabilized with PBS containing 0.1% Triton X-100 for 7 min, then washed in three washes of ice-cold PBS for 10 min each. The cells were blocked with 1% BSA in PBST for 1 h at room temperature, followed by incubation with *anti*-SLC4A11-Customized polyclonal antibody generated in rabbit against C-terminal of human SLC4A11 (IIEAKYLDVMDAEH) [37] overnight at 4 °C. Thereafter, the cells were washed in ice-cold PBS, incubated with secondary antibody for 1 h at room temperature in the dark, and rinsed three times in ice-cold PBS. The cells plated on the coverslips were mounted with a drop of mountant (#36984, Thermo Fisher Scientific) and examined by Zeiss Apotome microscope (Zeiss, Oberkochen, Germany).

4.4. Mitochondria isolation from cultured cells

90% confluent cells were washed twice with PBS, scraped with a cell lifter, and then pelleted by centrifugation at 500g for 5 min. The supernatant was discarded, and the cell pellet was incubated with mitochondrial isolation buffer (IB-1; 10 mM Tris-MOPS, 1 mM EGTA-Tris, 200 mM Sucrose, pH 7.4) for 10 min on ice. The cells were homogenized with pre-cooled glass Dounce homogenizer, followed by centrifugation at 1000 g for 10 min at 4 °C. The pellet containing unbroken cells and nuclei was discarded. The supernatant was centrifuged at 12,000 g for 15 min at 4 °C. The pellet containing mitochondria was washed with ice-cold IB-1, centrifuged at 12,000 g for 10 min at 4 °C, and collected into isotonic mitochondrial buffer (IB-2; 10 mM Tris-MOPS, 200 mM Sucrose, pH 7.4). The supernatant was saved as cytosolic fraction indicator. The protein concentrations of resuspended mitochondria were quantified using a BCA assay (#23225, Thermo Fisher Scientific).

4.5. Immunoblot analysis

15 μg of Mitochondrial lysates and supernatant fraction (cytosolic) were resolved by 7% SDS-PAGE for higher molecular proteins and 12% SDS-PAGE for small molecular proteins, then transferred to polyvinylidene difluoride membrane (PVDF). Membranes were blocked with 5% nonfat dried milk in TBST, incubated overnight at 4 °C with the indicated primary antibodies (HA epitope, BioLegend, 1:1000 dilution), SLC4A11 [37] (Custom, 1:500), TOM20 (SCBT, 1:1000), TIM23 (BD, 1:1000), VDAC (CST, 1:1000), UCP2 (CST, 1:1000), GLS1 (CST, 1:1000), Cytochrome c (Abcam, 1:1000), and α-tubulin (SCBT, 1:1500), washed three times in TBST (138 mM NaCl, 20 mM Tris, and 0.5% Tween 20, pH 7.6) for 10 min each, and incubated with secondary antibodies for 1 h at room temperature. After washing the membrane with TBST three times for 10 min each, the immunoreactive bands were visualized by enhanced chemiluminescence, ECL buffer (#34578, Thermo Fisher Scientific) using Gel Doc XR + system (Bio-Rad, Hercules, CA).

4.6. Digitonin treatment

Digitonin was dissolved in ddH_2O by heating to 95–98 °C and then cooled to room temperature. The isolated mitochondria (1 mg/ml) were incubated in 500 μl of ice-cold IB-2 at increasing concentrations of digitonin with gentle agitation on ice for 30 min. Immediately, 3 vol of ice-cold IB-2 were added and the sample centrifuged at 12,000 g for 10 min at 4 °C. The supernatant was saved and the pellet was washed twice in ice-cold IB-2 and finally resuspended with 100 μl of ice-cold IB-2. Mitochondrial lysates and supernatant fraction (15 μg) were analyzed by SDS-PAGE. Densitometric quantitative analysis of triplicate independent experiments was conducted using ImageJ to evaluate ratio of supernatant to total OMM (TOM20 and VDAC), IMM (TIM23 and UCP2) markers, and SLC4A11 (or SLC4A11-HA) vs. [Digitonin] in isolated mitochondria from HCEC and PS120-hSLC4A11-HA. Graphs depict mean ± SEM.

4.7. Transmission Electron Microscopy of isolated mitochondria

Isolated mitochondria from the cultured cells were fixed in 2% paraformaldehyde (#15700, EMS) and 0.25% glutaraldehyde (#16000, EMS) for 1 h at 4 °C, and centrifuged at 12,000 g for 10 min at 4 °C. The pellet was resuspended in 10 μl of 2% liquid agarose in PBS. After solidification, the specimens were fixed again in 2% paraformaldehyde and 0.25% glutaraldehyde for 30 min at 4 °C. The fixed specimens in agarose were dehydrated through an increased ethanol series, and infiltrated in a series of increasing LR White resin (#14381, EMS) and decreasing ethanol at 4 °C. The samples were placed in gelatin capsule and polymerized at 60 °C for 24 h. Sections were cut on a

ultramicrotome (Leica, Buffalo Grove, IL, USA) and placed on 300 mesh nickel grids (#EMS300-Ni, EMS). The sections were labelled with a combination of *anti*-SLC4A11 and anti-TOM20 for overnight at 4 °C and incubated with two different secondary antibodies conjugated to different sizes of colloidal gold particles (10 nm; goat-*anti*-rabbit against *anti*-SLC4A11 (#25109, EMS), and 25 nm goat-*anti*-mouse against anti-TOM20 (#25136, EMS)). Thereafter, the sections were washed on large droplets of 0.1% Tween 20 in PBS. The rinsed sections were stained with 2% uranyl acetate for 5 min in the dark, rinsed in H_2O, and then observed under a JEOL JEM 1010 transmission electron microscope (JEOL, Peabody, MA, USA).

4.8. Live tissue fluorescence microscopy

Freshly dissected corneas from WT and KO mice were obtained immediately after euthanasia. The endothelial surface was stained with MitoSOX (#M36008, Thermo Fisher Scientific) 2.5 μM in HBSS for 20 min at 37 °C and washed 3 times for 15 min in HBSS. Corneas were positioned with endothelial surface facing down in a glass bottom 35 mm Petri dish (#P35G-1.5-20-C, MatTek.Ashland, MA, USA). Confocal images were taken with a Leica SP5 Scanning Confocal Microscope (Leica, Buffalo Grove, IL, USA). Integrated pixel intensity was calculated with ImageJ.

In separate experiments, excised mouse corneas were incubated with MitoTracker Green FM (#M7514, Thermo Fisher Scientific) 1 μM in HBSS and incubated 15 min at 37 °C and washed 3 times for 15 min in HBSS. Corneas were positioned with endothelium facing down. Super resolution images were acquired with a Delta-Vision OMX microscope (GE Healthcare, USA). Whole cell thickness (4 μm) was acquired in 33 sections. Structured illumination analysis was performed with Worx software (Softworx, Montana, USA). Mitochondrial morphology analysis was performed with Mitochondrial Network Analysis Tool (MINA) [51] from ImageJ.

4.9. Acute measure of mitochondrial membrane potential

MCECs were cultured on fibronectin precoated 25-mm diameter glass coverslips (GG-25-pdl; Neuvitro Corporation, Vancouver, WA, USA) for 2–3 days. TMRE fluorescence was measured in non-quenching mode. Before each experiment, cells were incubated with TMRE 30 nM in Bicarbonate-free Ringer (5.5 mM glucose) for 30 min at 37 °C. Coverslips with subconfluent cells were mounted into a perfusion chamber, and the chamber was then placed on a stage warmer (37 °C) of an inverted microscope (Eclipse TE200; Nikon, Tokyo, Japan). For freshly dissected mouse corneas, they were placed in a perfusion chamber with endothelium facing the objective. Cells and tissues were perfused with a Bicarbonate-free Ringer containing TMRE (10 nM), equilibrated with air, pH adjusted to 7.5 with 1 N NaOH at 37 °C. Perfusing solutions were kept at 37 °C in a warming box, and the flow of the perfusate (~0.5 mL/min) was by gravity. Once a stable baseline fluorescence was achieved, perfusing solution was switched to Ringer containing 25 mM NH_4Acetate. Osmolarity of all solutions was adjusted to 295 mOsm with sucrose. Cells were imaged with a 40x oil-immersion objective (Nikon), corneas were imaged with a 40X water immersion LWD objective (Nikon). TMRE fluorescence was excited at 554 ± 10 nm and the emitted light was collected through a bandpass filter (570–635 nm). Fluorescence excitation and emission collection was controlled by a PTI RatioMaster (Horiba Scientific).

Flow Cytometry for Apoptosis, MMP, and mitoROS.

MCEC cultures in 12-well format were trypsinized and washed. Cultures were stained in triplicate with AnV-FITC + PI (#K101-100, Biovision Inc, Milpitas, CA, USA) for 5 min at room temperature; or with Tetramethylrhodamine Ethyl Ester Percholate (TMRE) (#T669, Thermo Fisher Scientific) 100 nM for 30 min at 37 °C; or with MitoSOX (#M36008, Thermo Fisher Scientific) 2.5 μM for 20 min a 37 °C, followed by one wash with HBSS. Cells were filtered in 50 μm sterile CellTrics Filters (#04-004-2327, Sysmex, Gorlitz, Germany) and collected in 5 ml FACS tubes. Cells were analyzed in FACSCalibur (BD Biosciences, San Jose, CA, USA) and 10,000 cells were collected per acquisition. Data was analyzed with FlowJo software (FlowJo, LLC, Ashland, OR, USA).

4.10. Ammonia assay

MCEC seeded at 4.5×10^5/mL in 12-well plates were cultured to confluence, then incubated with DMEM (no glucose, no glutamine, no sodium pyruvate, no phenol red) (#A14430-01; Thermo Fisher Scientific, Canoga Park, CA, USA), supplemented with glucose 1 g/L (#A24940-01, Thermo Fisher Scientific), ± glutamine (0.5 or 2 mM) (#250030–081, Thermo Fisher Scientific) and 0.5% dialyzed FBS (#26400–036) at 37 °C for 2–24 h. Medium supernatant after centrifugation was measured for ammonia concentration with an enzymatic colorimetric assay kit (K370-100, Biovision). When testing effect of Dimethyl-α-Ketoglutarate or Methyl-pyruvate a non-enzymatic method (K470-100) was used as both compounds highly interfere with the enzymatic assay. The non-enzymatic method requires sample-deproteinization that was achieved with 10 kD Spin Columns (#1997–25, Biovision).

4.11. ATP assay

MCEC after the incubation procedure mentioned above, were lysed in RIPA Buffer (#9806, Cell Signaling) plus PMSF (#8553, Cell Signaling) and ATP was immediately measured by luciferin-luciferase based ATP assay kit (A22066, Molecular Probes) in a microplate reader. Results were normalized to protein measured by BCA assay (#23225, Thermo Fisher Scientific).

4.12. Oxygen consumption Mito Stress Test

Cells were seeded in FNC-coated 8-well Miniplates (Agilent, #103025–100) in complete medium containing 14 mM Glucose and 4 mM Glutamine and incubated overnight at 37 °C in 5% CO_2 incubator. For experiments testing the effect of Glucose only, cells were incubated in complete medium without glutamine for 18 h. Medium was then changed to XF Base Medium (Agilent #102353–100) containing Glucose 14 mM ± Glutamine 4 mM and cells were incubated for 45 min at 37 °C (no CO_2). Mito Stress Kit for Seahorse XFp (Agilent, 103010–100) was used for preparing solutions in XF Base Medium for cartridge. Concentrations: Oligomycin 2 μM, FCCP 0.5 μM, Rotenone 0.5 μM and Antimycin A: 0.5 μM. Data analysis was performed with Wave Software and Multi-File Report Generator. Parallel wells were seeded for cell counting in Cellometer. Oxygen consumption rates were normalized by cell number.

4.13. Colocalization of MitoTracker and lysotracker analysis

MCEC WT or KO cells were plated on Fibronectin coated glass coverslips. They were grown in complete media (8% FBS) for 24 h followed by assay media (0.5 mM Gln, 5 mM Glucose and 0.5% dialyzed-FBS) addition for 4 h. Lysotracker Red DND (L7528, Thermo Fisher Scientific) (100 nM) and Mitotracker Green FM (#M7514, Thermo Fisher Scientific) (300 nM) were added to these cells and incubation was carried out at 37 °C following manufacturer's instructions (Thermo Fisher, Waltham, MA). Coverslips were washed in PBS, mounted on glass slides for imaging using Zeiss Apotome microscope (Zeiss, Oberkochen, Germany). All images were acquired at 40X, and were processed using Zen Pro software. Colocalization measurements were made as outlined: (https://www.zeiss.com/content/dam/Microscopy/Downloads/Pdf/FAQs/zen-aim_colocalization.pdf).
Briefly, to set up the threshold for co-localization measurements, images of single stained cells with either lysotracker red or Mitotracker

green were used. The average intensity of the respective channels (either red or green) were measured for at least 25 cells, and this value was used to set up the crosshairs for measuring the co-localization. At least 35 cells were outlined for all the samples, and the average Pearson's colocalization coefficients and their standard error were calculated. Statistical significance was calculated using unpaired t-tests. Statistical analyses were conducted using Graph Pad Prism software (La Jolla, CA).

4.14. Autophagy flux

MCEC WT and KO cells were grown in 12 well plates with complete media for 24 h. Assay media (with or without glutamine) was added to the cells for 4 h ± 1 μM Bafilomycin A1. Cells were lysed in RIPA buffer containing protease/phosphatase inhibitors. 20 μg of proteins were used for Western Blotting of LC3b and β-Actin.

4.15. Mitochondrial/nuclear DNA ratio

QPCR of beta-2 microglobulin (B2M) and mtDNA using primers from [52] (mtDNA 125 bp & nb2M 177 bp). Mito primers are designated in the area that does not show copies in nuclear DNA [52].

4.16. Mouse eye drop treatment

The effect of Dimethyl-α-Ketoglutarate on corneal thickness was tested by topical application. One drop (10 μl) of Dimethyl-α-Ketoglutarate (#349631: Sigma-Aldrich) 50 mM, in Lacripure saline solution (Menicon America Inc.) was applied to the right eye (OD) and one drop of Lacripure saline control solution to the left eye (OS) three times per day to *Slc4a11*$^{-/-}$ and *Slc4a11*$^{+/+}$ mice at 12 weeks of age (n = 3 for each condition, 12 mice total). Osmolarity was adjusted to 320 mOsm with Sucrose and solutions were sterilized by filtration. Central Corneal Thickness was measured using Optical Coherence Tomographer iVue100 (Optovue, Inc., Fremont,CA, USA) before treatment and weekly until the treatment was ended at 28 days.

4.17. Carcinoma cell siRNA knockdown

4.17.1. Cell culture

The human colon carcinoma cell lines HCT116 and HT29 were a gift from Heather O'Hagan, Medical Genetics IU School of Medicine. The cells were cultured in McCoy's5a medium (#10-050-CV, Corning) containing antibiotics and 3% (v/v) fetal bovine serum (HyClone) at 37 °C and incubated in a humidified 5% (v/v) CO_2 incubator. Cells were used at passage 9–20 in all experiments.

4.17.2. siRNA transfection

Human SLC4A11 siRNA was obtained from QIAGEN (#S104345278, Qiagen). The sequences of the siRNA duplex are 5′-ACACGAUUGUGAACGUGAATT-3' (sense) and 5′-UUCACGUUCACA AUCGUGUCA-3' (antisense). A non-targeting scrambled sequence siRNA (#SI001, Sigma-Aldrich) was used as control. HCT116 and HT29 cells were seeded in 12-well plates 24 h before transfection at a density of 1.5×10^5 cells/well in 1 ml medium. At ~60% confluency, the cells were transfected with 50 nM SLC4A11 siRNA or scrambled siRNA using HiPerFect reagent (#301705, Qiagen) per manufacturer's instruction. Thereafter, the cells were collected at different time points for subsequent protein expression and cell proliferation analyses.

4.17.3. SLC4A11 CRISPR KO in HCEC

SLC4A11 was disrupted in the Human corneal endothelial cell line by CRISPR/Cas9 plus HDR recombination technology. Briefly, HCEC were co-transfected with a plasmid containing gRNA targeting *SLC411* gene and Cas9 nuclease (sc-418241, Santa Cruz); along with a plasmid guiding HDR recombination in this region that contains Puromycin resistance and Red Fluorescent Protein (RFP) (sc-418241-HDR, Santa Cruz). Recombinant colonies were selected by puromycin. Red fluorescent cells were single cell cloned in 96 well plates by sorting with FACSAriaIIu (BD Biosciences). Clones were analyzed for efficient knock out by PCR of genomic DNA and RT-PCR of cDNA.

4.18. Statistical analysis

All flow cytometry measurements were performed in triplicate and repeated three times on different days. Other measures were performed at least three times unless otherwise noted. Error bars represent ± SEM. Statistical analysis was performed using SPSS Statistics v21 (IBM Corporation) and GraphPad Prime 6.0c (GraphPad Software, Inc.). Student t-test was used for two-group comparison. One-way ANOVA with post-hoc Tukey multiple comparison test was used for data with more than two groups. Significance was defined as $p < 0.05$.

Conflicts of interest

The authors have declared that no conflict of interest exists.

Author contributions

J.A.B. and D.O. designed the research plan and interpreted experimental results. D.O. performed all OCR, flow cytometry, and *in vivo* experiments. M.C. designed and executed mitochondrial localization imaging. R.S. performed autophagy experiments and oxidative stress imaging. S.L. designed and performed carcinoma experiments. JAB wrote and all authors helped edit the manuscript.

Acknowledgements

We thank Jason Tennessen and Brett Graham for helpful insights and suggestions; Barry Stein IUB EM facility; Christiane Hassel, Indiana University Flow Cytometry Core Facility; Jim Powers, Indiana University Light Microscopy Imaging Center; Matthew James Repass, Angio BioCore, IU Simon Cancer Center; Mallika Valapala, help with autophagy flux; and Edward T. Kim, technical assistance.

Appendix A. Supplementary data

Supplementary data to this article can be found online at https://doi.org/10.1016/j.redox.2019.101260.

Funding

NIH NEI/5R01EY008834 (JAB). RS is an Indiana University CTSI Postdoctoral Fellow NIH/NCATS CTSI TL1 TR002531 and UL1 TR002529.gs1

Conflicts of interest

None.

Data and materials availability

All data is available in the main text or the supplementary materials.

References

[1] B.J. Altman, Z.E. Stine, C.V. Dang, From Krebs to clinic: glutamine metabolism to cancer therapy, Nat. Rev. Canc. 16 (10) (2016) 619–634.
[2] W. Zhang, H. Li, D.G. Ogando, S. Li, et al., Glutaminolysis is essential for energy production and ion transport in human corneal endothelium, EBioMedicine 16 (2017) 292–301.
[3] S. Dasarathy, R.P. Mookerjee, V. Rackayova, V. Rangroo Thrane, et al., Ammonia toxicity: from head to toe? Metab. Brain Dis. 32 (2) (2017) 529–538.

[4] A. Adlimoghaddam, M.G. Sabbir, B.C. Albensi, Ammonia as a potential neurotoxic factor in alzheimer's disease, Front. Mol. Neurosci. 9 (2016) 57.
[5] G. Davuluri, A. Allawy, S. Thapaliya, J.H. Rennison, et al., Hyperammonaemia-induced skeletal muscle mitochondrial dysfunction results in cataplerosis and oxidative stress, J. Physiol. 594 (24) (2016) 7341–7360.
[6] A.R. Jayakumar, K.V. Rama Rao, A. Schousboe, M.D. Norenberg, Glutamine-induced free radical production in cultured astrocytes, Glia 46 (3) (2004) 296–301.
[7] V.G. Grivennikova, G. Cecchini, A.D. Vinogradov, Ammonium-dependent hydrogen peroxide production by mitochondria, FEBS Lett. 582 (18) (2008) 2719–2724.
[8] M.J. Hogan, J.A. Alvarado, J. Weddell, Histology of the Human Eye, W.B. Saunders, Philadelphia, 1971.
[9] S. Li, E. Kim, J.A. Bonanno, Fluid transport by the cornea endothelium is dependent on buffering lactic acid efflux, Am. J. Physiol. Cell Physiol. 311 (1) (2016) C116–C126.
[10] W. Zhang, D.G. Ogando, J.A. Bonanno, A.G. Obukhov, Human SLC4A11 is a novel NH3/H+ Co-transporter, J. Biol. Chem. 290 (27) (2015) 16894–16905.
[11] L. Kao, R. Azimov, X.M. Shao, R.F. Frausto, et al., Multifunctional ion transport properties of human SLC4A11: comparison of the SLC4A11-B and SLC4A11-C variants, Am. J. Physiol. Cell Physiol. 311 (5) (2016) C820–C830.
[12] W. Zhang, D.G. Ogando, E.T. Kim, M.J. Choi, et al., Conditionally immortal Slc4a11-/- mouse corneal endothelial cell line recapitulates disrupted glutaminolysis seen in Slc4a11-/- mouse model, Investig. Ophthalmol. Vis. Sci. 58 (9) (2017) 3723–3731.
[13] X. Jiao, A. Sultana, P. Garg, B. Ramamurthy, et al., Autosomal recessive corneal endothelial dystrophy (CHED2) is associated with mutations in SLC4A11, J. Med. Genet. 44 (1) (2007) 64–68.
[14] S.B. Han, H.P. Ang, R. Poh, S.S. Chaurasia, et al., Mice with a targeted disruption of Slc4a11 model the progressive corneal changes of congenital hereditary endothelial dystrophy, Investig. Ophthalmol. Vis. Sci. 54 (9) (2013) 6179–6189.
[15] S. Guha, S. Chaurasia, C. Ramachandran, S. Roy, SLC4A11 depletion impairs NRF2 mediated antioxidant signaling and increases reactive oxygen species in human corneal endothelial cells during oxidative stress, Sci. Rep. 7 (1) (2017) 4074.
[16] U.V. Jurkunas, M.S. Bitar, T. Funaki, B. Azizi, Evidence of oxidative stress in the pathogenesis of fuchs endothelial corneal dystrophy, Am. J. Pathol. 177 (5) (2010) 2278–2289.
[17] J.D. Gottsch, A.L. Bowers, E.H. Margulies, G.D. Seitzman, et al., Serial analysis of gene expression in the corneal endothelium of Fuchs' dystrophy, Investig. Ophthalmol. Vis. Sci. 44 (2) (2003) 594–599.
[18] S.S. Jalimarada, D.G. Ogando, J.A. Bonanno, Loss of ion transporters and increased unfolded protein response in Fuchs' dystrophy, Mol. Vis. 20 (2014) 1668–1679.
[19] G.L. Vilas, S.K. Loganathan, A. Quon, P. Sundaresan, et al., Oligomerization of SLC4A11 protein and the severity of FECD and CHED2 corneal dystrophies caused by SLC4A11 mutations, Hum. Mutat. 33 (2) (2012) 419–428.
[20] E.J. Myers, A. Marshall, M.L. Jennings, M.D. Parker, Mouse Slc4a11 expressed in Xenopus oocytes is an ideally selective H+/OH- conductance pathway that is stimulated by rises in intracellular and extracellular pH, Am. J. Physiol. Cell Physiol. 311 (6) (2016) C945–C959.
[21] S.K. Loganathan, C.M. Lukowski, J.R. Casey, The cytoplasmic domain is essential for transport function of the integral membrane transport protein SLC4A11, Am. J. Physiol. Cell Physiol. 310 (2) (2016) C161–C174.
[22] B.J. Berry, A.J. Trewin, A.M. Amitrano, M. Kim, et al., Use the protonmotive force: mitochondrial uncoupling and reactive oxygen species, J. Mol. Biol. 430 (21) (2018) 3873–3891.
[23] R.J. Mailloux, M.E. Harper, Uncoupling proteins and the control of mitochondrial reactive oxygen species production, Free Radic. Biol. Med. 51 (6) (2011) 1106–1115.
[24] K. Alka, J.R. Casey, Ophthalmic nonsteroidal anti-inflammatory drugs as a therapy for corneal dystrophies caused by SLC4A11 mutation, Investig. Ophthalmol. Vis. Sci. 59 (10) (2018) 4258–4267.
[25] E. Verdin, NAD(+) in aging, metabolism, and neurodegeneration, Science 350 (6265) (2015) 1208–1213.
[26] M.P. Langford, J.M. Gosslee, C. Liang, D. Chen, et al., Apical localization of glutamate in GLAST-1, glutamine synthetase positive ciliary body nonpigmented epithelial cells, Clin. Ophthalmol. 1 (1) (2007) 43–53.
[27] Y. Wang, Y. Nartiss, B. Steipe, G.A. McQuibban, et al., ROS-induced mitochondrial depolarization initiates PARK2/PARKIN-dependent mitochondrial degradation by autophagy, Autophagy 8 (10) (2012) 1462–1476.
[28] D.J. Klionsky, K. Abdelmohsen, A. Abe, M.J. Abedin, et al., Guidelines for the use and interpretation of assays for monitoring autophagy (3rd edition), Autophagy 12 (1) (2016) 1–222.
[29] X. Li, P. Fang, J. Mai, E.T. Choi, et al., Targeting mitochondrial reactive oxygen species as novel therapy for inflammatory diseases and cancers, J. Hematol. Oncol. 6 (2013) 19.
[30] B.M. Kenwood, J.L. Weaver, A. Bajwa, I.K. Poon, et al., Identification of a novel mitochondrial uncoupler that does not depolarize the plasma membrane, Mol. Metab. 3 (2) (2014) 114–123.
[31] A.V. Zhdanov, A.H. Waters, A.V. Golubeva, R.I. Dmitriev, et al., Availability of the key metabolic substrates dictates the respiratory response of cancer cells to the mitochondrial uncoupling, Biochim. Biophys. Acta 1837 (1) (2014) 51–62.
[32] M. Skowronska, J. Albrecht, Oxidative and nitrosative stress in ammonia neurotoxicity, Neurochem. Int. 62 (5) (2013) 731–737.
[33] K. Qureshi, K.V. Rao, I.A. Qureshi, Differential inhibition by hyperammonemia of the electron transport chain enzymes in synaptosomes and non-synaptic mitochondria in ornithine transcarbamylase-deficient spf-mice: restoration by acetyl-L-carnitine, Neurochem. Res. 23 (6) (1998) 855–861.
[34] A.V. Kareyeva, V.G. Grivennikova, G. Cecchini, A.D. Vinogradov, Molecular identification of the enzyme responsible for the mitochondrial NADH-supported ammonium-dependent hydrogen peroxide production, FEBS Lett. 585 (2) (2011) 385–389.
[35] H. Cheong, T. Lindsten, J. Wu, C. Lu, et al., Ammonia-induced autophagy is independent of ULK1/ULK2 kinases, Proc. Natl. Acad. Sci. U. S. A. 108 (27) (2011) 11121–11126.
[36] L. Qin, T. Li, Y. Liu, High SLC4A11 expression is an independent predictor for poor overall survival in grade 3/4 serous ovarian cancer, PLoS One 12 (11) (2017) e0187385.
[37] D.G. Ogando, S.S. Jalimarada, W. Zhang, E.N. Vithana, et al., SLC4A11 is an EIPA-sensitive Na(+) permeable pHi regulator, Am. J. Physiol. Cell Physiol. 305 (7) (2013) C716–C727.
[38] T. Litman, R. Sogaard, T. Zeuthen, Ammonia and urea permeability of mammalian aquaporins, Handb. Exp. Pharmacol. 190 (2009) 327–358.
[39] L. Kao, R. Azimov, N. Abuladze, D. Newman, et al., Human SLC4A11-C functions as a DIDS-stimulatable H(+)(OH(-)) permeation pathway: partial correction of R109H mutant transport, Am. J. Physiol. Cell Physiol. 308 (2) (2015) C176–C188.
[40] S.K. Loganathan, H.P. Schneider, P.E. Morgan, J.W. Deitmer, et al., Functional assessment of SLC4A11, an integral membrane protein mutated in corneal dystrophies, Am. J. Physiol. Cell Physiol. 311 (5) (2016) C735–C748.
[41] Y.H. Ko, Z. Lin, N. Flomenberg, R.G. Pestell, et al., Glutamine fuels a vicious cycle of autophagy in the tumor stroma and oxidative mitochondrial metabolism in epithelial cancer cells: implications for preventing chemotherapy resistance, Cancer Biol. Ther. 12 (12) (2011) 1085–1097.
[42] L.M. Harder, J. Bunkenborg, J.S. Andersen, Inducing autophagy: a comparative phosphoproteomic study of the cellular response to ammonia and rapamycin, Autophagy 10 (2) (2014) 339–355.
[43] C.H. Eng, K. Yu, J. Lucas, E. White, et al., Ammonia derived from glutaminolysis is a diffusible regulator of autophagy, Sci. Signal. 3 (119) (2010) ra31.
[44] S. Kitajima, K.L. Lee, H. Hikasa, W. Sun, et al., Hypoxia-inducible factor-1alpha promotes cell survival during ammonia stress response in ovarian cancer stem-like cells, Oncotarget 8 (70) (2017) 114481–114494.
[45] N.M. Cetinbas, J. Sudderth, R.C. Harris, A. Cebeci, et al., Glucose-dependent anaplerosis in cancer cells is required for cellular redox balance in the absence of glutamine, Sci. Rep. 6 (2016) 32606.
[46] C. Hurtaud, C. Gelly, Z. Chen, C. Levi-Meyrueis, et al., Glutamine stimulates translation of uncoupling protein 2mRNA, Cell. Mol. Life Sci. 64 (14) (2007) 1853–1860.
[47] A. Vozza, G. Parisi, F. De Leonardis, F.M. Lasorsa, et al., UCP2 transports C4 metabolites out of mitochondria, regulating glucose and glutamine oxidation, Proc. Natl. Acad. Sci. U. S. A. 111 (3) (2014) 960–965.
[48] S. Siddiqui, J.C. Zenteno, A. Rice, O. Chacon-Camacho, et al., Congenital hereditary endothelial dystrophy caused by SLC4A11 mutations progresses to Harboyan syndrome, Cornea 33 (3) (2014) 247–251.
[49] M.D. Parker, E.P. Ourmozdi, M.J. Tanner, Human BTR1, a new bicarbonate transporter superfamily member and human AE4 from kidney, Biochem. Biophys. Res. Commun. 282 (5) (2001) 1103–1109.
[50] T. Schmedt, Y. Chen, T.T. Nguyen, S. Li, et al., Telomerase immortalization of human corneal endothelial cells yields functional hexagonal monolayers, PLoS One 7 (12) (2012) e51427.
[51] A.J. Valente, L.A. Maddalena, E.L. Robb, F. Moradi, et al., A simple ImageJ macro tool for analyzing mitochondrial network morphology in mammalian cell culture, Acta Histochem. 119 (3) (2017) 315–326.
[52] A.N. Malik, A. Czajka, P. Cunningham, Accurate quantification of mouse mitochondrial DNA without co-amplification of nuclear mitochondrial insertion sequences, Mitochondrion 29 (2016) 59–64.